ELSEVIER

Journal of Membrane Science 212 (2003) 177–193

journal of MEMBRANE SCIENCE

www.elsevier.com/locate/memsci

# Heat transport and membrane distillation coefficients in direct contact membrane distillation

J. Phattaranawik [a], R. Jiraratananon [a,*], A.G. Fane [b]

[a] *Department of Chemical Engineering, King Mongkut's University of Technology Thonburi, Toongkru, Bangkok 10140, Thailand*
[b] *UNESCO Centre for Membrane Science & Technology, School of Chemical Engineering and Industrial Chemistry, The University of New South Wales, Sydney, NSW 2052, Australia*

Received 20 June 2002; received in revised form 25 September 2002; accepted 11 October 2002

**Abstract**

This work aims to provide detailed understanding of heat transport in direct contact membrane distillation (DCMD). The influence of mass transfer on heat transfer rates and on the heat transfer coefficient was identified, and the relative significance of each heat transfer mechanism was evaluated. The role of spacers in heat transfer improvement was analyzed. Alternative methods to evaluate the membrane thermal conductivity were also proposed.

The heat transfer analysis of the experimental results showed that the effects of mass transfer on the heat transfer rates and on the film heat transfer coefficients were negligible. The heat transfer due to the vapor flow ($q_v$) in the membrane was equal to or greater than the heat conduction ($q_c$) for the membranes studied and increased with the feed temperature. When the feed temperature was lower than 323 K, the heat loss due to heat conduction across the membrane was the major contribution of the total heat transfer in the membrane. In addition, the temperature distributions in the membranes were closely linear. The membrane distillation (MD) coefficients for each membrane were constant over the flow rates and temperatures studied. The flow pattern in the spacer-filled channel was probably transition flow rather than turbulent flow. The alternative models for calculating the membrane thermal conductivity showed better agreement than the commonly used model.


*Keywords:* Effect of mass transfer; Heat transport; Membrane distillation; Membrane distillation coefficient; Spacers

## 1. Introduction

Membrane distillation (MD) is a hybrid process that uses membranes and operates on the basis of evaporation. Unlike most other membrane processes, MD does not require a mechanical pressure pump and is not limited by the osmotic pressure. In MD, mass is transported by the difference in vapor pressures between feed and permeate. The most common configuration of MD is direct contact membrane distillation (DCMD) in which both heated feed and cold permeate streams are in direct contact with the porous, hydrophobic membrane. The difference in the temperature and composition of solutions in the layers adjoining the membrane between the feed and permeate streams creates the vapor pressure driving force for DCMD. On the other hand, the chemical potential resulting from the temperature difference plays an important role in both heat and mass transport. The DCMD process takes place at atmospheric pressure and at temperatures that are much lower than the normal boiling point of the feed solutions. The vaporization at the hot

* Corresponding author. Tel.: +66-2-470-9222; fax: +66-2-428-3534.
*E-mail address:* ratana.jir@kmutt.ac.th (R. Jiraratananon).

0376-7388/02/$ – see front matter 
PII: S0376-7388(02)00498-2

**Nomenclature**

| | |
|---|---|
| $C$ | membrane distillation coefficient ($kg\,m^{-2}\,s^{-1}\,Pa^{-1}$) |
| $C_{pv}$ | specific heat of vapor ($kJ\,kg^{-1}\,K^{-1}$) |
| $d_f$ | filament size (m) |
| $d_{h,s}$ | hydraulic diameter of spacer-filled channel (m) |
| $D$ | hydraulic diameter of empty channel (m) |
| $h$ | heat transfer coefficient for low mass transfer rate ($W\,m^{-2}\,K^{-1}$) |
| $h^*$ | heat transfer coefficient for high mass transfer rate ($W\,m^{-2}\,K^{-1}$) |
| $h_f$ and $h_p$ | heat transfer coefficients at feed and permeate sides |
| $H$ | spacer thickness (m) |
| $H_v\{T\}$ | vapor enthalpy at temperature $T$ ($kJ\,kg^{-1}$) |
| $J$ | mass flux ($kg\,m^{-2}\,s^{-1}$) |
| $k$ | thermal conductivity coefficient ($W\,m^{-1}\,K^{-1}$) |
| $k_{dc}$ | correction factor for spacer |
| $l_m$ | mesh size (m) |
| $Nu$ | Nusselt number |
| $Pr$ | Prandlt number |
| $q_c$ | heat transfer by conduction |
| $q_f$ and $q_p$ | convective heat transfer rates across the boundary layer at feed and permeate sides ($kW\,m^{-2}$) |
| $q_f^m$ and $q_p^m$ | heat transfer rates due to mass transfer across the thermal boundary layers of feed and permeate sides ($kW\,m^{-2}$) |
| $q_v$ | heat transfer due to vapor flowing through the membrane ($kW\,m^{-2}$) |
| $Re$ | Reynolds number |
| $T_1$ and $T_2$ | temperatures at membrane surface on feed and permeate sides (K) |
| $T_f$ and $T_p$ | bulk temperatures of feed and permeate (K) |

*Greek letters*

| | |
|---|---|
| $\delta$ | membrane thickness |
| $\varepsilon$ | membrane porosity |
| $\theta$ | spacer hydrodynamic angle |
| $\tau$ | temperature polarization coefficient |
| $\varphi$ | spacer voidage |
| $\phi$ | rate factor |
| $\psi_T$ | correction factor of high mass transfer rate effect for heat transfer |

*Subscripts*

| | |
|---|---|
| g | air |
| m | membrane |
| s | solid |
| foil | aluminum foil |

feed–membrane surface interface produces the vapor, which is then driven across the membrane by various mass transport mechanisms, and condenses at the membrane surface–cold permeate solution interface. The hydrophobicity of the membrane protects against liquid penetration through the membrane. Thus, only vapor or gas phase is allowed to enter the membrane pores.

The heat transfer with simultaneous mass transfer takes place in DCMD, resulting in complex heat transfer mechanisms. As a consequence, the mass transfer can affect both heat transfer rates and heat transfer coefficients [1,2]. The heat transfer model has been proposed to describe the heat transfer mechanisms in DCMD and facilitates the evaluation of the membrane surface temperatures. In most literatures, the heat transfer model for DCMD was developed based on the assumption of linear temperature profile and isenthalpy flow of vapor. However, there are different heat transfer models derived based on other assumptions. Gryta and Tomaszewska [3] derived the heat transfer model by assuming non-isenthalpy flow of vapor and non-linear temperature distribution and used the temperature on membrane surface on the permeate side as thermodynamic reference temperature. Although better agreement between the measured mass fluxes and the predicted fluxes was achieved, the significance of each heat transfer mechanism was not mentioned. Izquierdo-Gil et al. [4] achieved the heat transfer model from the conservation of enthalpy flux and the terms of heat flux due to mass flux were first introduced to MD. Both works showed better agreements between experimental and calculation results. However, the previous models did not mention the details and importance of heat

transfer mechanisms involved. Furthermore, such models cannot identify the influence of mass transfer on heat transfer rates. Recently, Phattaranawik and Jiraratananon [5] proposed the heat transfer model that can identify the influence of mass transfer on heat transfer rates and significance of each heat transfer mechanism in DCMD. However, the experimental data employed in [5] were taken from Lawson and Lloyd's work [6], which covered only turbulent flow condition and one membrane material (polypropylene). In addition, the thermal conductivity of the membrane used in the calculation was too low, $0.024\,W\,m^{-1}\,K^{-1}$ [5,6]. Hence, the calculation results did not cover all membrane material and flow conditions.

Spacers may be applied as the turbulent promoter in DCMD to increase both heat and mass transfer [7,8]. The maximum flux enhancement was obtained by approximately 50%. On the other hand, the spacers in the UF processes improved fluxes by three- to five-fold [9,10]. In addition, turbulent or upper transition flow regime was found in the spacer-filled channels for UF and RO [9,11] although the Reynolds numbers were still in laminar regime. However, the flow characteristic for spacer-filled channels in DCMD has not been investigated.

From above discussion, the influence of mass transfer on heat transfer rates and on heat transfer coefficients for DCMD was ignored in most works. However, high mass transfer rate theory [1,2] suggests that high mass transfer rates have strong effect on heat transport, especially the transfer coefficients (momentum, heat, and mass). In addition, the significance of each heat transfer mechanism has not been described clearly. Accordingly, the understanding in the heat transfer of DCMD is still incomplete.

This paper intends to illustrate the details of all heat transfer mechanisms in feed stream, inside the membrane, and in permeate stream. The main objectives of this work are to: (1) study the effect of mass transfer on heat transfer rates and heat transfer coefficients; (2) determine the significance of each heat transfer mechanism for both laminar and turbulent flow conditions; (3) prove the validity of the assumptions of linear temperature profile inside the membrane and isenthalpic flow of vapor; (4) identify the flow condition in spacer-filled channels.

## 2. Theory

### 2.1. Heat transfer model and temperature distribution inside the membrane

The heat transfer in DCMD relies on the complex relation between simultaneous heat and mass transfer, which are transported in the same direction from hot feed to cold permeate. The schematic diagram of heat and mass transfer for DCMD is illustrated in Fig. 1. The difference between the bulk temperatures and the temperatures at the liquid–vapor interface or membrane surfaces on both sides of the membrane is termed temperature polarization, which appears in all configurations of membrane distillation. The temperature polarization coefficient [12] defined in Eq. (1) is used to measure the magnitude of this phenomenon. Furthermore, the temperature polarization can be regarded as a defect of the DCMD process, which should be minimized. The use of spacers, as the turbulent promoters [7,8], and turbulent flow [6] are appropriate methods to decrease the effect of this phenomenon.

$$\tau = \frac{T_1 - T_2}{T_f - T_p} \tag{1}$$

$T_1$ and $T_2$ are the membrane surface temperatures on the heated feed and cold permeate sides, respectively, whereas $T_f$ and $T_p$ are the bulk temperatures of feed and permeate streams. The temperature polarization coefficient is, therefore, the ratio of the actual driving force to the overall driving force.

Mass transport across the membrane in DCMD is generally described by various mass transfer models based on the dusty gas model [13], such as the Knudsen model, the Poiseuille model, the

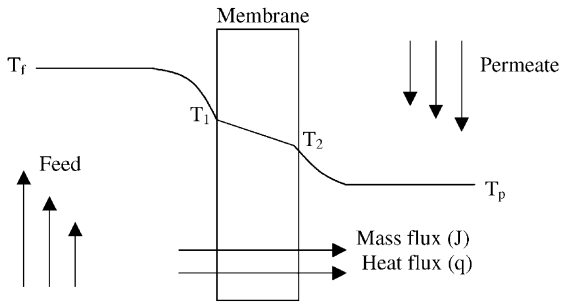


Fig. 1. Heat and mass transfer in DCMD.

Knudsen–Poiseuille transition models, and the molecular diffusion model [6,12,14]. The selection of the most appropriate model depends on the properties of vapor and membrane, i.e. the mean free path and mean pore size. However, in most cases, the models suggest that the mass flux may be written as a linear function of the vapor pressure difference across the membrane, given by

$$J = C(P_1 - P_2) \tag{2}$$

where $J$ is the mass flux, $C$ the membrane distillation coefficient, and $P_1$ and $P_2$ the partial pressure of vapor (water) at the membrane surfaces on the feed and permeate sides, respectively. According to the mass transfer models, the membrane distillation coefficient ($C$) is a function of the membrane properties (pore size, thickness, porosity, and membrane tortuosity), properties of the vapor transported across the membrane (molecular weight and diffusivity), and temperatures.

The original expression for heat transfer with simultaneous mass transfer is derived from energy conservation [1,2], Eq. (3)

$$q = JH\{T\} - k\frac{\mathrm{d}T}{\mathrm{d}X} \tag{3}$$

where $q$ is the total heat flux, $J$ the mass flux, $H\{T\}$ the enthalpy at temperature $T$, $k$ the thermal conductivity, and $x$ the distance in direction of heat transfer. In addition, the term for convective heat transfer should replace the conduction term in Eq. (3) to illustrate the heat transport in the feed and permeate streams. Thus, Eq. (3) becomes Eq. (4)

$$q = JH\{T\} + h(T_{\mathrm{bulk}} - T_{\mathrm{sur}}) \tag{4}$$

where $h$ is the convective heat transfer coefficient, $T_{\mathrm{bulk}}$ the bulk temperature, and $T_{\mathrm{sur}}$ the surface temperature.

As seen in Fig. 1, energy transport in DCMD is divided into three regions; feed, membrane, and permeate regions. The mechanisms of heat transfer in the feed and permeate streams can be described by Eq. (4), and Eq. (3) is used to explain the heat transfer across the membrane. The heat transfer model [5] can be visualized by the electrical analog shown in Fig. 2. The heat transfer in each region with model elements were mentioned in our previous work [5].

To achieve the temperature distribution inside the membrane, the heat transfer mechanisms in the membrane have to be considered. The heat transport across the membrane ($q_{\mathrm{m}}$) can be divided in to two possible mechanisms, conduction across the membrane material ($q_{\mathrm{c}}$) together with a heat due to vapor flowing through the membrane ($q_{\mathrm{v}}$). With the assumption of non-linear temperature distribution and non-isenthalpic flow, the heat transfer equation inside the membrane is given by

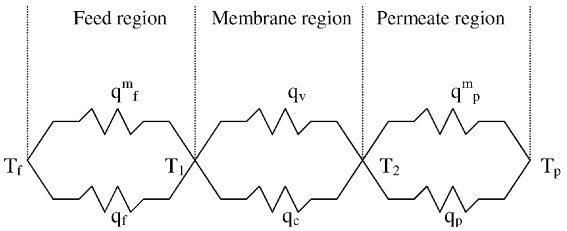


Fig. 2. The electrical analogy of heat transfer model for DCMD.

$$q_{\mathrm{m}} = JH_{\mathrm{v}}\{T\} - k_{\mathrm{m}}\frac{\mathrm{d}T}{\mathrm{d}X} \tag{5}$$

where $H_{\mathrm{v}}\{T\}$ is the vapor enthalpy at temperature $T$, and $k_{\mathrm{m}}$ is the thermal conductivity of the membrane that is contributed from both polymer material ($k_{\mathrm{s}}$) and gases ($k_{\mathrm{g}}$) which are usually air and water vapor. In some cases, the presence of vapor mixtures, for example acid or alcohol vapor mixed up with water vapor, causes problems in calculating $k_{\mathrm{g}}$ because it is difficult to approximate the mole fraction of each vapor in the membrane. In the case of the air–water vapor mixture, there is a small difference between their thermal conductivities. Consequently, the mixture can be assumed to be a single component (air).

Generally, the reference temperature ($T_0$) is 273 K, so $H_{\mathrm{v}}\{T\}$ can be written in the forms below

$$H_{\mathrm{v}}\{T\} = C_{\mathrm{pv}}T + (H_{\mathrm{v}}\{T_0\} - C_{\mathrm{pv}}T_0) \tag{6}$$

Here, $C_{\mathrm{pv}}$ is specific heat of vapor and liquid, and $H_{\mathrm{v}}\{T_0\}$ is vapor enthalpy evaluated at the reference temperature, $T_0$.

By assuming that $k_{\mathrm{m}}$ is constant over the range of temperatures considered with steady-state conditions, both heat and mass flux are constant in all regions. The temperature distribution in the membrane is obtained by substituting Eq. (6) into Eq. (5), separating the variables, and integrating the equation for the boundary conditions, $x = 0$, $T = T_1$ and $x = x$, $T = T$. The

expression representing the temperature distribution in the membrane is shown in Eq. (7).

$$T = (\alpha + T_1)\exp(\gamma x) - \alpha \tag{7}$$

where

$$\alpha = \frac{JH_v\{T_0\} - q_m - JC_{pv}T_0}{JC_{pv}} \tag{8}$$

and

$$\gamma = \frac{JC_{pv}}{k_m} \tag{9}$$

The term $\gamma x$ represents the ratio of heat transport contributed by mass transfer inside the membrane to heat conduction through the membrane. Eq. (7) also reveals that the temperature profile in the membrane is an exponential function of the distance ($x$) due to the assumption of non-isenthalpic flow of water vapor. Although the positive sign of $\gamma x$ gives an increasing function with distance, the value of $\alpha$ calculated by Eq. (8) is negative which results in decreasing temperatures across the membrane evaluated by Eq. (7). The typical values of $\alpha$ and $\gamma$ are approximately $-2000$ K and 70 $m^{-1}$ (at $T_f = 323$ K, GVHP membrane, and laminar flow). At $x = \delta$ (membrane thickness), $T = T_2$ and the equation used to calculated $q_m$ in Eq. (8) appears in Eq. (10)

$$q_m = \frac{C_{pv}JT_1\exp(\gamma\delta) - C_{pv}JT_2}{\exp(\gamma\delta) - 1} + J(H_v\{T_0\} - C_{pv}T_0) \tag{10}$$

At steady-state conditions, heat fluxes in each region are transported with identical rates, which allows us to obtain the expressions that can be used to evaluate the membrane surface temperatures ($T_1$ and $T_2$), details are given in [5].

### 2.2. The influence of mass transfer on heat transfer rate and significance of each heat transfer mechanism

The significance of the mechanisms is determined after the membrane surface temperatures $T_1$ and $T_2$ are obtained from the heat transfer model. The mass fluxes are obtained from the experimental measurements, and the heat transfer coefficients are calculated from the heat transfer correlations for heat exchangers. The methods to calculate the effect of mass transfer on heat transfer in the feed and the permeate streams ($q_f^m$ and $q_p^m$) were described in [5]. The heat transfer due to vapor flowing through the membrane ($q_v$) is calculated by

$$q_v = JH_v\{T\} \tag{11}$$

The heat conduction across the membrane can be determined from the difference between $q_m$ and $q_v$. The membrane distillation coefficients are calculated by Eq. (2), and the vapor pressures of water at the membrane surface temperatures are calculated by the Antoine equation for water. In addition, the enthalpies of water vapor and liquid are determined from the equations fitted from the enthalpy data of saturated water vapor and liquid taken from the thermodynamic property table [15,16] in the range of temperature 273–373 K, expressed as

$$H_v\{T\} = 1.7535(T) + 2024.3 \tag{12}$$

where $H$ is in kJ $kg^{-1}$, and $T$ in K.

### 2.3. Thermal conductivity of membrane

As mentioned previously, the thermal conductivity of the membrane is contributed from both polymer ($k_s$) and air ($k_g$). For homopolymers, $k_s$ is mainly dependent upon the temperature, spatial arrangement, the degree of crystallinity and shape of the crystallites [17,18]. However, the thermal conductivity of crystalline polymers is a weak function of temperature because the polymer chains in crystalline structure hardly move or vibrate when energy is absorbed. For instance, the thermal conductivities for polyvinylidenedifluoride (PVDF), polytetrafluoroethylene (PTFE), and polypropylene (PP) tested by the standard method ASTM C177, are reported in a narrow range: PVDF 0.17–0.19 W $m^{-1}$ $K^{-1}$ (at 296 K) and 0.21 W $m^{-1}$ $K^{-1}$ (at 348 K); PTFE 0.25–0.27 W $m^{-1}$ $K^{-1}$ (at 296 K) and 0.29 W $m^{-1}$ $K^{-1}$ (at 348 K); PP 0.11–0.16 W $m^{-1}$ $K^{-1}$ (at 296 K) and 0.2 W $m^{-1}$ $K^{-1}$ (at 348 K) [19–21]. The thermal conductivities of air and water vapor are reported as 0.026 W $m^{-1}$ $K^{-1}$ (at 298 K) and 0.03 W $m^{-1}$ $K^{-1}$ (at 348 K) for air, and 0.020 W $m^{-1}$ $K^{-1}$ (at 298 K) and 0.022 W $m^{-1}$ $K^{-1}$ (at 348 K) [22] for water vapor. Fortunately, there is a very small difference between the thermal conductivities of vapor and air. Thus, it is

possible to assume that the gases in the pores behave as one component.

There are three models that can be used to predict the thermal conductivity of two-phase composite material, based on molecular orientation: (1) the Isostrain or parallel model [23] (Eq. (13)); (2) Isostress or series model [23] (Eq. (14)); (3) flux law model [24] (Eq. (15)).

Isostrain model:

$$k_m = (1-\varepsilon)k_s + \varepsilon k_g \tag{13}$$

Isostress model:

$$k_m = \left[\frac{\varepsilon}{k_g} + \frac{(1-\varepsilon)}{k_s}\right]^{-1} \tag{14}$$

Flux law model:

$$k_m = k_g\left[\frac{1+(1-\varepsilon)\beta_{s-g}}{1-(1-\varepsilon)\beta_{s-g}}\right] \tag{15}$$

where

$$\beta_{s-g} = \frac{k_s/k_g - 1}{k_s/k_g + 2}$$

where $\varepsilon$ is membrane porosity. Eq. (13) is often utilized for MD, and Eqs. (14) and (15) are the alternative expressions to calculate the membrane thermal conductivity.

### 2.4. The influence of mass transfer on heat transfer coefficient

Transfer of mass across the thermal boundary layers possibly distorts the temperature profiles in the thermal boundary layers [1,2] of both feed and permeate streams. Generally, convective heat transfer correlations are developed based on the assumption of small rate of mass transfer, Eq. (16). When a high rate of mass transfer exists in the system being considered, all transfer coefficients (momentum, heat, and mass) depend on the mass transfer rate (Eq. (17)) [1].

$$Nu = f(Re, Pr, \text{ channel geometry}) \tag{16}$$

$$Nu = f\left(Re, Pr, \frac{J_A C_{pA} + J_B C_{pB}}{h}, \text{channel geometry}\right) \tag{17}$$

The effect of high mass transfer on film heat transfer coefficients can be assessed by the correction factor ($\psi_T$) in Eq. (18) [1,2], which may be evaluated by the film theory or the penetration theory, and the boundary layer theory. However, only the film theory is discussed in this work due to its simple solution, Eqs. (18) and (19)

$$\psi_T = \frac{h^*}{h} = \frac{\phi}{\exp(\phi) - 1} \tag{18}$$

where

$$\phi = -\frac{J_A C_{pA}}{h} \tag{19}$$

In Eq. (19), $\phi$, $J_A$, $C_{pA}$, and $h$ are the rate factor, the molar flux, the heat capacity of species A, and heat transfer coefficient at low mass transfer calculated by ordinary Nusselt number correlations, respectively. $h^*$ in Eq. (18) is the apparent heat transfer coefficient including the effect of high mass transfer rates. The minus sign in Eq. (19) is due to the water removed from the feed side [1,2]. The typical values of $\psi_T$ are estimated in Section 4.3.

### 2.5. The spacers for DCMD

Net-type spacers are often put into the flow channels in membrane processes such as reverse osmosis and ultrafiltration to improve the mass transfer and to reduce the effect of concentration polarization and fouling [9,25]. Spacer geometry and the flow moving through the spacer is shown in Fig. 3. Spacers also have benefits in MD [7,8] since they destabilize the flow and create eddy currents in the laminar regime so that momentum, heat, and mass transfer are enhanced.

The heat transfer correlation for DCMD with spacers was obtained from the mass transfer correlation for UF [26] under the assumed analogy between heat and mass transfer

$$Nu = k_{dc} 0.664\, Re_s^{0.5}\, Pr^{0.33}\left(\frac{2d_{h,s}}{l_m}\right)^{0.5} \tag{20}$$

where

$$k_{dc} = 1.654\left(\frac{d_f}{H}\right)^{-0.039}\varphi^{0.75}\left(\sin\left(\frac{\theta}{2}\right)\right)^{0.086}$$

Here, $k_{dc}$ is the correction factor for spacer geometry, $d_{h,s}$ the hydraulic diameter for the spacer-filled channel, $d_f$ filament size, $l_m$ the mesh size, $H$ the spacer

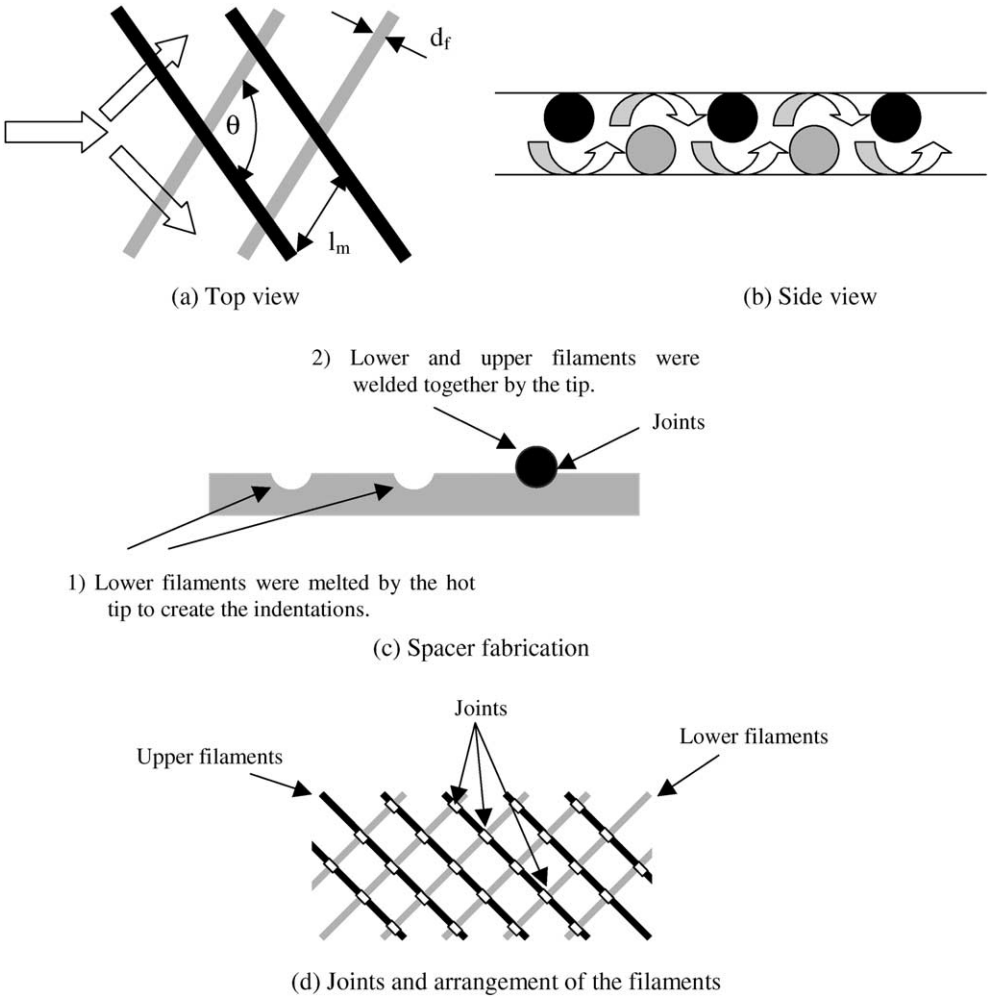


Fig. 3. Flow direction in spacer-filled channel and spacer fabrication.

thickness, $\varphi$ the spacer voidage, and $\theta$ the hydrodynamic angle. In this work, DCMD experiments with the spacers were carried out to identify the flow conditions in the spacer-filled channels.

## 3. Experimental

The membrane modules for laminar and turbulent flow conditions were made from polymethylmethacrylate (PMMA). The dimensions and the characteristics of both modules are shown in Table 1. In the experiments, both modules were placed in the vertical position in order to eliminate the effects of free convection. Distilled water was used as the feed and permeate solutions. The membranes used were PVDF (nos. 1 and 2), and PTFE (no. 3), and their reported properties are summarized in Table 2. In addition, membranes nos. 4 and 5 are also included for the discussion in Section 4.1.

The feed solution was heated and maintained at the required temperature in a 28 l thermostatic water bath (Nickel-Electro: model NE4D) with sensitivity ±0.1 K and uniformity ±0.01 K. The low temperature circulator for the permeate solution was supplied by Vision Scientific (model VS-1205CW) with

Table 1
Membrane module characteristics and channel dimensions

| Membrane module | Width (m) | Length (m) | Height (m) | Hydraulic diameter of channel (m) | Effective membrane area ($m^2$) |
|---|---|---|---|---|---|
| Laminar flow | $5 \times 10^{-2}$ | $1 \times 10^{-1}$ | $5 \times 10^{-3}$ | $9.09 \times 10^{-3}$ | $5 \times 10^{-3}$ |
| Turbulent flow | $3 \times 10^{-3}$ | $1 \times 10^{-1}$ | $3 \times 10^{-3}$ | $3 \times 10^{-3}$ | $3 \times 10^{-4}$ |

Table 2
Membrane properties [4]

| No. | Membrane material | Pore size (μm) | Thickness (μm) | Porosity ($\varepsilon$) | $k_{m,r}$ ($W\,m^{-1}\,K^{-1}$) | Manufacturer |
|---|---|---|---|---|---|---|
| 1 | PVDF (GVHP) | 0.22[a] | 126 | 0.62 | 0.041 | Millipore |
| 2 | PVDF (HVHP) | 0.45[a] | 116 | 0.66 | 0.040 | Millipore |
| 3 | PTFE | 0.2[a] | 70 | 0.7[a] | – | Sartorious |
| 4 | PTFE | 0.2[a] | 64 | 0.9 | 0.031 | Gore |
| 5 | PTFE | 0.45[a] | 77 | 0.89 | 0.027 | Gore |

Note: $k_{m,r}$ are the reported membrane thermal conductivities [4]; GVHP and HVHP are code names of the PVDF membranes produced by Millipore.
[a] Manufacturer's data.

uniformity ±0.1 K. The feed and permeate solutions were pumped co-currently into the top of the modules by precision brushless drives (model 7741) supplied by Cole-Parmer (Master Flex), and the flow rates were measured by a glass variable area flow meter (model 10A1197) supplied by ABB Fisher & Porter for the hot feed stream and by a polycarbonate flow meter (model RMB-85) provided by Dwyer for the cold permeate stream. The solution temperatures were measured by digital thermometers supplied by Testo (model Testo 935). The process solutions were circulated through closed thermostatic systems. The bulk temperatures of feed solutions were varied from 313 to 343 K with 10 K increments, and the permeate temperatures were constant at 293 K.

The experiments were divided into three parts. (1) The experiments for obtaining the most suitable heat transfer correlations for laminar and turbulent flow modules used. (2) DCMD experiments were performed with the empty channels. The measured mass fluxes at various operating conditions were used to calculate the influence of mass transfer on heat transfer rates and on heat transfer coefficients, to assess the significance of each heat transfer mechanism, and to evaluate the membrane distillation coefficient ($C$). (3) DCMD experiments with two types of the spacers to identify the flow characteristic in the spacer-filled channel and study the enhancement of heat and mass transfer by the spacers.

### 3.1. Determination of appropriate heat transfer correlations

To eliminate the mass transfer, the membranes were replaced by the aluminum foil with thickness of 40 μm and thermal conductivity of 229 $W\,m^{-1}\,K^{-1}$. In this part, Reynolds numbers for both sides were kept equal, and the experiments were conducted with four different flow rates ($Re$), shown in Table 3. The calculated overall heat transfer coefficients from the heat transfer correlations ($U_{corre}$, Eq. (21)) and the experimental overall heat transfer coefficient ($U_{exp}$, Eq. (22)) were compared, and standard deviations [27] of the differences were considered to determine the best heat transfer correlation for each flow condition

$$U_{corre} = \frac{1}{[(1/h_h) + (\delta_{foil}/k_{foil}) + (1/h_c)]} \quad (21)$$

Table 3
The experimental conditions for determining the appropriate heat transfer correlations

| Temperature (K) | | Reynolds numbers | |
|---|---|---|---|
| Feed | Permeate | Laminar | Turbulent |
| 313–343 | 293 | 762 | 12,217 |
| 313–343 | 293 | 1142 | 15,708 |
| 313–343 | 293 | 1523 | 17,453 |
| 313–343 | 293 | 2094 | 19,198 |

Table 4
Heat transfer correlations for laminar flow

| Correlation | | Reference |
|---|---|---|
| $Nu = 1.86\left(\frac{Re\,Pr}{L/D}\right)^{1/3}$ | (23) | [28] |
| $Nu = 4.36 + \frac{0.036 Re\,Pr(D/L)}{1 + 0.0011(Re\,Pr(D/L))^{0.8}}$ | (24) | [3] |
| $Nu_{cooling} = 11.5(Re\,Pr)^{0.23}(D/L)^{0.5}$, $Nu_{heating} = 15(Re\,Pr)^{0.23}(D/L)^{0.5}$ | (25) | [27] |
| $Nu = 0.13 Re^{0.64}\,Pr^{0.38}$ | (26) | [27] |
| $Nu = 1.95\left(\frac{Re\,Pr}{L/D}\right)^{1/3}$ | (27) | [29][a] |
| $Nu = 0.097 Re^{0.73}\,Pr^{0.13}$ | (28) | [27] |
| $Nu = 3.66 + \frac{0.104 Re\,Pr(D/L)}{1 + 0.0106(Re\,Pr(D/L))^{0.8}}$ | (29) | [29] |

[a] Average Nusselt number.

$$U_{exp} = \frac{Q}{A\,\Delta T_{ln}} \tag{22}$$

where

$$\Delta T_{ln} = \frac{(T_{h,in} - T_{c,in}) - (T_{h,out} - T_{c,out})}{\ln[(T_{h,in} - T_{c,in})/(T_{h,out} - T_{c,out})]}$$

In Eqs. (21) and (22), $Q$ is the heat transfer rate, $\delta_{foil}$ the foil thickness, $k_{foil}$ the foil thermal conductivity, $h_h$ the heat transfer coefficient of hot solution, and $h_c$ the heat transfer coefficient of the cold solution. The heat transfer correlations tested for both flow conditions are shown in Tables 4 and 5.

In Tables 4 and 5, $L$ is the channel length and $D$ the hydraulic diameter of the membrane module. The entrance effect term, $(1 + (6D/L))$ [34], is considered for most correlations in Table 5. The most appropriate heat transfer correlations obtained were used to evaluate the heat transfer coefficients in the subsequent experiments.

### 3.2. The DCMD experiments with the empty channels

The same heat transfer coefficients for both feed and permeate streams were employed in order to compare the effect of mass transfer on each side. However, the same flow rates cannot provide the same heat transfer coefficients due to the large difference between the bulk feed and permeate temperatures. Accordingly, the flow rates of the feed side were reset in order to equalize the heat transfer coefficients of both sides. The chosen correlations from Section 3.1 were used to calculate both the experimental conditions (fluid velocity) and the heat transfer coefficients. The experiments for this part were performed with three different flow rates (heat transfer coefficients) for each flow condition, shown in Table 6.

### 3.3. The DCMD experiments with spacer-filled channels

The operating conditions used in this part were similar to those previously described for laminar flow conditions (Table 6) except that spacers were put in both feed and permeate channels. To minimize the bypass flow the spacer thickness was equal to the channel height, that is, 5 mm for both spacers. The spacers were made 'in house' from polypropylene rod 3 mm in diameter. A welding rod with a sharp tip was electrically heated and used to fabricate the spacers. Spacer thickness ($H$) should be less than double the filament diameters since vertically directional flow change is required (see Fig. 3b). The hot tip was used to create indents of approximately 1 mm in the lower filaments. Then, the upper filaments were placed across the indents and the tip was used to weld both filaments together (see Fig. 3c). The welding positions and arrangement of upper and lower filaments are displayed in Fig. 3d. Dimensional errors in fabricating spacers were controlled to levels less than 8% (Table 7). The relationship in Eq. (37) [26] was used to evaluate the mesh size ($l_m$) at the required voidage ($\varphi$) and hydrodynamic angle ($\theta$). Both voidage and mesh size are necessary for spacer fabrication. The geometric characteristics of the spacers are summarized in Table 7.

$$l_m = \frac{\pi d_f^2}{2(1-\varphi)H\sin\theta} \tag{37}$$

In Eq. (37) $d_f$ is the diameter of the spacer filament and $H$ the spacer thickness. The mass fluxes obtained from the experiments with spacers were compared to those from the experiments performed under laminar and turbulent flow conditions so as to estimate the heat transfer coefficients and identify the flow characteristic for spacer-filled channels.

Table 5
Heat transfer correlations for turbulent flow

| Correlation | | Reference |
|---|---|---|
| $Nu = \left(1 + \frac{6D}{L}\right)\left(\frac{(f/8)Re\,Pr}{1.07 + 12.7(f/8)^{1/2}(Pr^{2/3} - 1)}\right)$ | (30) | [29] |
| $Nu = \left(1 + \frac{6D}{L}\right)\left(\frac{(f/8)(Re - 1000)Pr}{1 + 12.7(f/8)^{1/2}(Pr^{2/3} - 1)}\right)$ | (31) | [30] |
| $Nu = 0.023\left(1 + \frac{6D}{L}\right)Re^{0.8}\,Pr^{1/3}$ | (32) | [31] |
| $Nu = 0.036\mathrm{Re}^{0.8}\,Pr^{1/3}\left(\frac{D}{L}\right)^{0.055}$ | (33) | [32] |
| $Nu = \left(1 + \frac{6D}{L}\right)\left(\frac{(f/8)Re\,Pr}{1.2 + 13.2(f/8)^{1/2}(Pr^{2/3} - 1)}\right)$ | (34) | [33] |
| $Nu = \left(1 + \frac{6D}{L}\right)\left(\sqrt{\frac{f}{8}}\right)\left[12.48Pr^{2/3} - 7.853Pr^{1/3} + 3.613\ln(Pr) + 5.8 + 2.78\ln\left(\frac{Re\sqrt{f/32}}{45}\right)\right]^{-1}$ | (35) | [33] |
| $Nu = 0.027\left(1 + \frac{6D}{L}\right)Re^{0.8}\,Pr^{1/3}\left(\frac{\mu_{bulk}}{\mu_{sur}}\right)^{0.14}$ | (36) | [32] |

Note: $f = (0.79\ln(Re) - 1.64)^{-2}$ for all correlations.

Table 6
Operating conditions and heat transfer coefficients calculated by Eq. (24) for laminar flow and by Eq. (32) for turbulent flow

| Run | Temperature (K) | | Laminar flow (Eq. (24)) | | | Turbulent flow (Eq. (32)) | | |
|---|---|---|---|---|---|---|---|---|
| | Feed | Permeate | Fluid velocity ($m\,s^{-1}$) | | Heat transfer coefficient ($W\,m^{-2}\,K^{-1}$) | Fluid velocity ($m\,s^{-1}$) | | Heat transfer coefficient ($W\,m^{-2}\,K^{-1}$) |
| | | | Feed | Permeate | | Feed | Permeate | |
| 1 | 313 | 293 | 0.063 | 0.063 | 1054.3 | 2.59 | 3.50 | 17,026.3 |
| 2 | 323 | 293 | 0.063 | 0.063 | 1054.3 | 2.32 | 3.50 | 17,026.3 |
| 3 | 333 | 293 | 0.060 | 0.063 | 1054.3 | 2.13 | 3.50 | 17,026.3 |
| 4 | 343 | 293 | 0.060 | 0.063 | 1054.3 | 1.94 | 3.50 | 17,026.3 |
| 5 | 313 | 293 | 0.083 | 0.084 | 1281.9 | 3.06 | 4.09 | 19,261.0 |
| 6 | 323 | 293 | 0.083 | 0.084 | 1281.9 | 2.78 | 4.09 | 19,261.0 |
| 7 | 333 | 293 | 0.083 | 0.084 | 1281.9 | 2.50 | 4.09 | 19,261.0 |
| 8 | 343 | 293 | 0.083 | 0.084 | 1281.9 | 2.22 | 4.09 | 19,261.0 |
| 9 | 313 | 293 | 0.100 | 0.105 | 1498.9 | 3.52 | 4.67 | 21,432.4 |
| 10 | 323 | 293 | 0.100 | 0.105 | 1498.9 | 3.14 | 4.67 | 21,432.4 |
| 11 | 333 | 293 | 0.100 | 0.105 | 1498.9 | 2.87 | 4.67 | 21,432.4 |
| 12 | 343 | 293 | 0.097 | 0.105 | 1498.9 | 2.59 | 4.67 | 21,432.4 |

Table 7
Characteristics of spacers

| No. | Voidage ($\varphi$) | Hydrodynamic angle ($\theta$) | Hydraulic diameter (m) | $l_m$ (m) |
|---|---|---|---|---|
| 1 | 0.612 | 45(±7%) | $2.7 \times 10^{-3}$(±5%) | $11 \times 10^{-3}$(±7%) |
| 2 | 0.623(±8%) | 90(±5%) | $2.8 \times 10^{-3}$(±5%) | $8 \times 10^{-3}$(±7%) |

Note: Spacer thickness = 5(±8%) mm.

## 4. Results and discussion

### 4.1. Thermal conductivities of the membranes

The values of $k_{m,r}$ taken from [4] were compared with the calculated membrane thermal conductivities ($k_{m,c}$) by various models. As shown in Table 8, the Isostress model, Eq. (14), provided the best agreement for all membranes. On the other hand, the Isostrain model (Eq. (13)) which is usually used to calculate the membrane thermal conductivity in most MD studies provided very large discrepancies. Therefore, the Isostress model (Eq. (14)) appeared to be the most appropriate model for calculating the membrane thermal conductivity, and also suggests that the thermal conductivity of the PTFE (no. 3) was 0.0382 $W m^{-1} K^{-1}$.

### 4.2. The most suitable heat transfer correlations

For repeated runs of each experiment, the measured temperatures: $T_{h,in}$, $T_{h,out}$, $T_{c,in}$, and $T_{c,out}$ fluctuated slightly within 4% of the average values (or ±0.8 K at 293 K). As a result, the average error of measured overall heat transfer coefficients was less than 7%. $U_{exp}$ ranged from 480 to 1240 $W m^{-2} K^{-1}$ for laminar flow and 7100–16,000 $W m^{-2} K^{-1}$ for turbulent flow. The thermal resistances of the foil were approximately 1.1% of the total resistance due to foil thinness and high thermal conductivity.

Table 9 compares the standard deviations of heat transfer correlations. The most suitable heat transfer correlations for each flow condition were chosen at the minimum standard deviation. Thus, Eq. (24) in Table 4 and Eq. (32) in Table 5 were selected for laminar flow and turbulent flow conditions, respectively. The average discrepancies between $U_{exp}$ and $U_{corre}$ calculated by the chosen correlations were about 6% for laminar flow and 9% for turbulent flow. Subsequently, the selected correlations were used to calculate the required operating conditions and to evaluate the corresponding convective heat transfer coefficients for both flow conditions (Table 6). It should be noted that high standard deviation was found for Eq. (23), which is the commonly used Seider–Tate equation for laminar flow. On the other hand, the commonly used Dittus–Boelt equation was the most suitable for turbulent condition.

### 4.3. The influence of mass transfer on heat transfer rates and heat transfer coefficients, significance of each heat transfer mechanism, and membrane distillation coefficients

The importance of each heat transfer mechanism was determined and interpreted in the forms of percentage compared to the total heat transfer rates. The influence of mass transfer on heat transfer rates was described by percentage of $q_f^m$ and percentage of $q_p^m$. As seen in Figs. 4 and 5, the maximum percentages at 343 K was 7.2% for $q_f^m$ and 2.8% for $q_p^m$. Both $q_f^m$ and $q_p^m$ increase with the feed temperatures due to higher mass fluxes. In Fig. 5, the heat transfer coefficients slightly affected both $q_f^m$ and $q_p^m$ because the increase of the heat transfer coefficients raised $q_f^m$ and $q_p^m$, and $q_f$ and $q_p$ in the same portions. The impact of mass transfer on the heat transfer coefficients in the feed stream can be assessed by the correction factor ($\psi_T$) calculated by Eqs. (18) and (19), and Fig. 16. For PTFE at 343 K, $\psi_T$ was approximately 1.009 for $h = 1054.29\ W m^{-2} K^{-1}$ and 1.0015 for $h = 21{,}432.4\ W m^{-2} K^{-1}$. As a result, the effect of mass transfer on the heat transfer coefficients was only 0.9 and 0.15% of the coefficients calculated by the

Table 8
Calculations of membrane thermal conductivities

| No. | Membrane | $k_{m,r}$ ($W m^{-1} K^{-1}$) | Isostrain model | | Isostress model | | Flux law model | |
|---|---|---|---|---|---|---|---|---|
| | | | $k_{m,c}$ ($W m^{-1} K^{-1}$) | Error (%) | $k_{m,c}$ ($W m^{-1} K^{-1}$) | Error (%) | $k_{m,c}$ ($W m^{-1} K^{-1}$) | Error (%) |
| 1 | PVDF | 0.041 | 0.0858 | 109.17 | 0.0412 | 0.56 | 0.046 | 12.55 |
| 2 | PVDF | 0.040 | 0.0797 | 99.20 | 0.0393 | 1.81 | 0.044 | 9.25 |
| 3 | PTFE | – | 0.0946 | – | 0.0382 | – | 0.044 | – |
| 4 | PTFE | 0.031 | 0.0502 | 61.94 | 0.0307 | 0.88 | 0.032 | 4.45 |
| 5 | PTFE | 0.027 | 0.0524 | 94.15 | 0.0310 | 14.93 | 0.033 | 21.69 |

Note: $k_s$ (polymer) = 0.18 and 0.25 $W m^{-1} K^{-1}$ for PVDF and PTFE, respectively; $k_g$ (air) = 0.028 $W m^{-1} K^{-1}$ for all calculations.

Table 9
Standard deviations of the heat transfer correlations

| | S.D. ($W\,m^{-2}\,K^{-1}$) |
|---|---|
| Laminar flow | |
| Eq. (23) | 314.72 |
| Eq. (24) | 53.69[a] |
| Eq. (25) | 252.04 |
| Eq. (26) | 57.58 |
| Eq. (27) | 290.49 |
| Eq. (28) | 71.87 |
| Eq. (29) | 171.96 |
| Turbulent flow | |
| Eq. (30) | 2196.33 |
| Eq. (31) | 2065.97 |
| Eq. (32) | 1334.81[a] |
| Eq. (33) | 1591.62 |
| Eq. (34) | 1634.49 |
| Eq. (35) | 1401.31 |
| Eq. (36) | 2157.94 |

[a] Minimum S.D.

correlations with no or low mass transfer, respectively. Under the condition of the calculation (PTFE at 343 K and turbulent condition) the mass fluxes were about $0.014\,kg\,m^{-2}\,s^{-1}$ ($50.4\,l\,m^{-2}\,h^{-1}$). Therefore, in this study the mass transfer in DCMD did not affect either heat transfer rates or heat transfer coefficients.

Figs. 6 and 7 show that the percentage of heat transfer due to vapor transport inside the membrane ($q_v$) varied from 40 to 62% for GVHP and also increased with the feed temperatures because of the higher mass fluxes. The similar trends were found for HVHP and

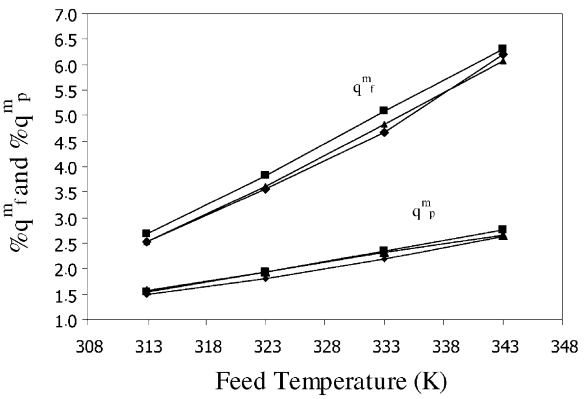


Fig. 4. Percentages of $q_f^m$ and $q_p^m$ at various feed temperatures for laminar flow, $h = 1498.87\,W\,m^{-2}\,K^{-1}$; (◆) GVHP 0.22 μm; (■) HVHP 0.45 μm; (▲) PTFE 0.2 μm.

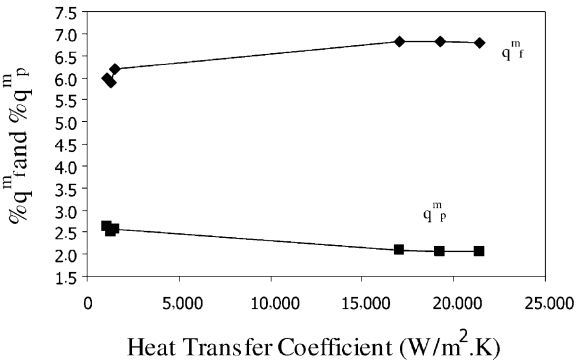


Fig. 5. Percentages of $q_f^m$ and $q_p^m$ at various heat transfer coefficients (flow rate, flow conditions), $T_f = 343\,K$, for GVHP 0.22 μm; (◆) $q_f^m$ and (■) $q_p^m$.

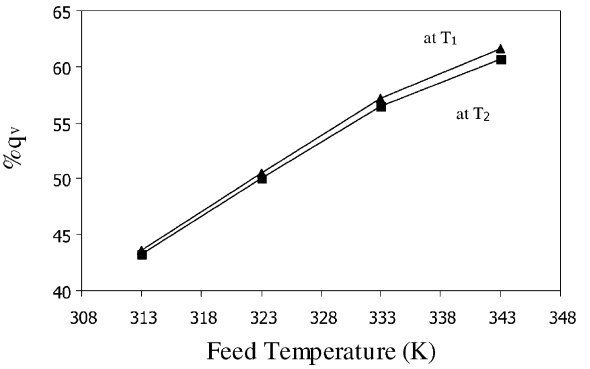


Fig. 6. Percentages of $q_v$ at various feed temperatures for HVHP 0.45 μm, $h = 1498.87\,W\,m^{-2}\,K^{-1}$.

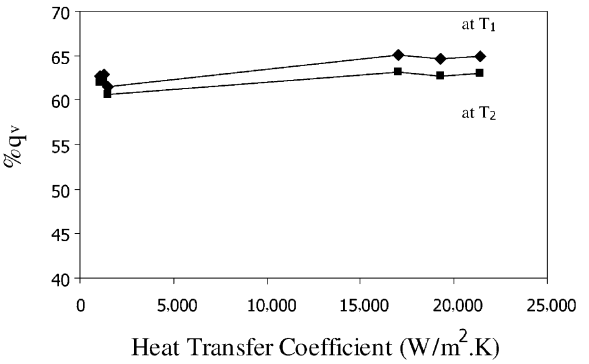


Fig. 7. Percentages of $q_v$ at various heat transfer coefficients (flow rate), $T_f = 343\,K$, for HVHP 0.45 μm.

PTFE with the maximum percentage of $q_v$ of 63.4% (PTFE and turbulent flow). In Fig. 7, the significance of $q_v$ seems independent of the film heat transfer coefficients used. Thus, the significance of $q_v$ was comparable to heat conduction across the membrane ($q_c$). Compared to the previous simulation [5], with polypropylene membranes, the maximum percentage of $q_v$ was 92% and $q_v$ was the major component of heat transfer inside the membranes, and the heat conduction ($q_c$) could be disregarded. $q_f^m$, $q_p^m$ and $q_v$ in present work were rather lower than those in the previous simulation [5] due to difference in the membrane materials and properties. However, the present results are judged to be more reasonable because of the use of the membrane properties experimentally determined [4]. Fig. 6 also reveals that the heat loss by heat conduction ($q_c$) was larger than $q_v$ when the feed temperature was lower than 323 K. To minimize the proportion of the heat loss in the membrane, higher feed temperature and low thermal conductivity membranes are required.

Figs. 8 and 9 reveal that the temperature polarization coefficients ($\tau$) for laminar and turbulent flow decreased with increasing feed temperature due to higher energy consumption from the vaporization at the feed membrane surface at higher temperatures. Significantly higher $\tau$ values for turbulent flow can be seen by comparing Figs. 8 and 9. This is illustrated more clearly in Fig. 10, which shows the effect of heat transfer coefficients (a flow regime) on $\tau$. The temperature polarization was reduced by higher flow rates due to the decrease in the thermal resistances of convection in the boundary layers.

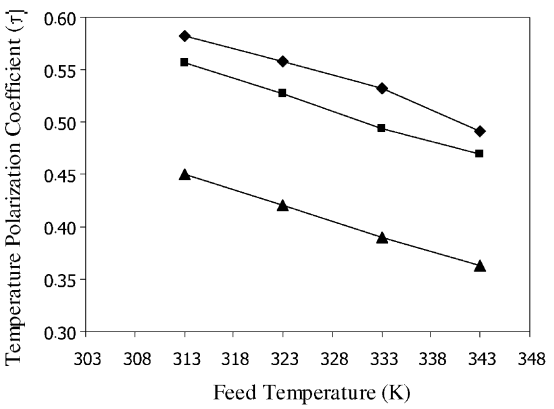


Fig. 8. Temperature polarization coefficients at various feed temperatures for laminar flow condition, $h = 1498.87\,W\,m^{-2}\,K^{-1}$; (◆) GVHP 0.22 μm; (■) HVHP 0.45 μm; (▲) PTFE 0.2 μm.

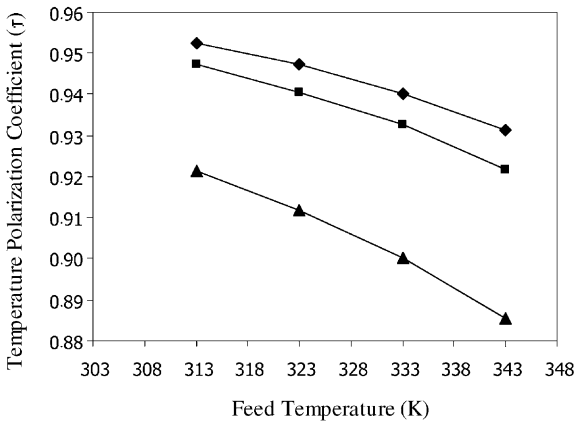


Fig. 9. Temperature polarization coefficients at various feed temperatures for turbulent flow condition, $h = 21{,}423.4\,W\,m^{-2}\,K^{-1}$; (◆) GVHP 0.22 μm; (■) HVHP 0.45 μm; (▲) PTFE 0.2 μm.

The membrane distillation coefficients ($C$) were evaluated by Eq. (2). The analysis results showed that MD coefficients were not affected by flow rates (heat transfer coefficients) and membrane temperatures studied (Fig. 11). The constant slopes of the straight lines in Fig. 11 mean the MD coefficients that are $3.459 \times 10^{-7}\,kg\,m^{-2}\,s^{-1}\,Pa^{-1}$ for GVHP, $4.169 \times 10^{-7}\,kg\,m^{-2}\,s^{-1}\,Pa^{-1}$ for HVHP, and $6.245 \times 10^{-7}\,kg\,m^{-2}\,s^{-1}\,Pa^{-1}$ for PTFE. The MD

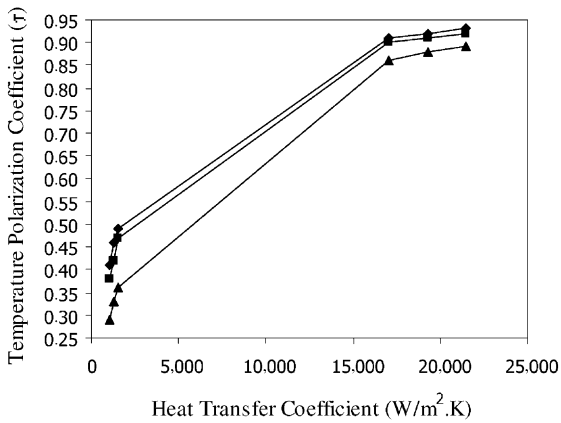


Fig. 10. Temperature polarization coefficients at various heat transfer coefficients (flow rates, flow conditions), $T_f = 343$ K; (◆) GVHP 0.22 μm; (■) HVHP 0.45 μm; (▲) PTFE 0.2 μm.

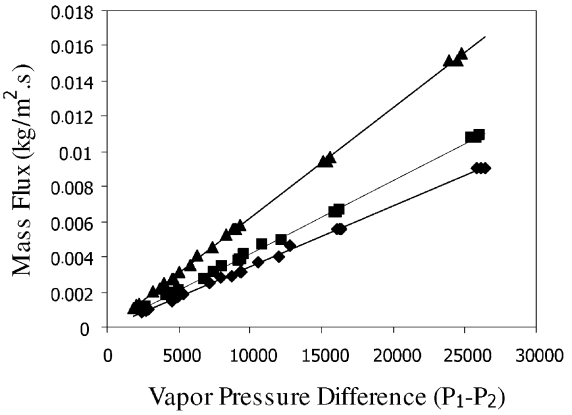


Fig. 11. Mass fluxes at various driving force; (◆) GVHP 0.22 μm; (■) HVHP 0.45 μm; (▲) PTFE 0.2 μm.

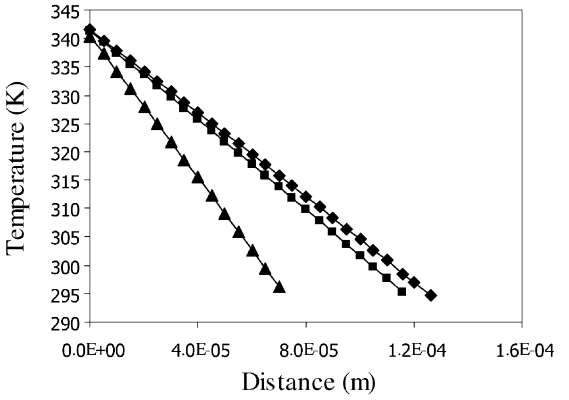


Fig. 12. Temperature distributions for each membrane at $T_f = 343$ K, $h = 21{,}423.4\,W\,m^{-2}\,K^{-1}$; (◆) GVHP 0.22 μm; (■) HVHP 0.45 μm; (▲) PTFE 0.2 μm.

coefficient for the HVHP is lower than that reported in the previous work [12] by 15.1% due to differences in the calculation methods. The MD coefficients as defined in Eq. (2) represent the mass transfer coefficient across the membrane region. As a result, changes in flow rates in feed and permeate streams should not affect MD coefficients. In the range of the membrane temperatures studied (303–318 K), the temperatures did not influence the MD coefficients. There are two possible reasons to explain why MD coefficients are not dependent on the temperatures. First, the change in the average membrane temperatures was less than 5% from 303 to 318 K. Second, the majority of mass transfer occurred within the transition region [6]. Consequently, the MD coefficients consist of two major contributions: a Knudsen diffusion part ($C_K$) that decreases with temperature to the power of −0.5 [12,14]and a molecular diffusion part ($C_M$), that increases with temperature to the power of 1.34 [6]. These components would counterbalance and therefore, the net values of MD coefficients were almost constant over the temperature range used in these experiments.

The temperature distributions inside the membranes were estimated by Eqs. (7)–(9). Fig. 12 shows the distributions of each membrane for turbulent flow condition, and the similar trends are obtained for laminar flow condition. Figs. 13 and 14 display the influence of the feed temperatures and flow rates on the temperature profiles, respectively. In Fig. 14, higher trans-membrane temperatures were obtained at higher flow rates leading to higher mass fluxes. Although the temperature profile is expressed in the form of an exponential function, the calculated temperature profiles are nearly linear for all membranes and experimental conditions studied. The possible reason is that the membranes are relatively thin (very short distance). Therefore, the assumption of the linear temperature profile in the membranes used in previous works [3,27] was valid.

If heat transfer due to mass transfer in the feed and permeate streams ($q_f^m$ and $q_p^m$) are neglected, the simplified equations to calculate the membrane surface temperatures are given by Eqs. (38) and (39). The

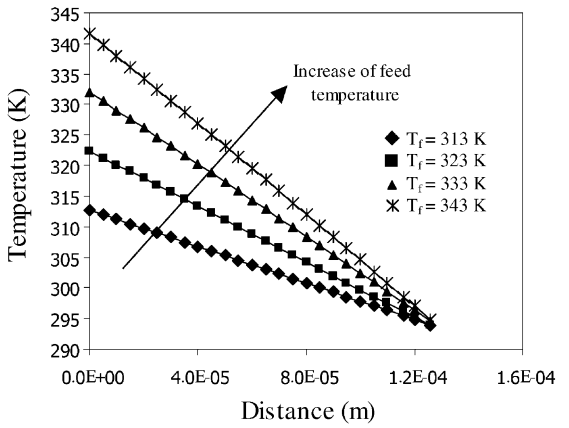


Fig. 13. Effect of feed temperatures on temperature distributions for GVHP, $h = 21{,}423.4\,W\,m^{-2}\,K^{-1}$.

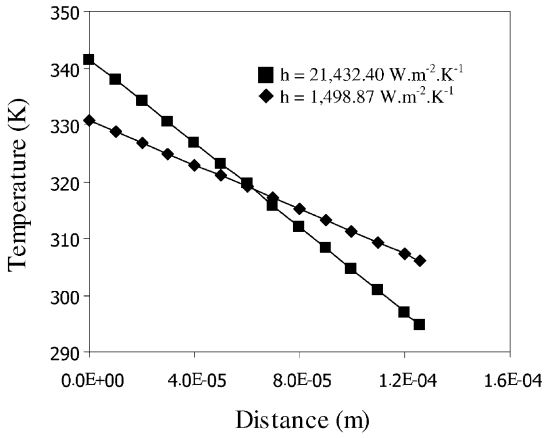


Fig. 14. Effect of film heat transfer coefficients (flow rates) on temperature distributions for GVHP.

arrangement in both expressions helps describe the phenomenon of polarization. The second terms in such expressions can be regarded as the polarization terms.

$$T_1 = T_f - \frac{q_v + q_c}{h_f} \tag{38}$$

$$T_2 = T_p + \frac{q_v + q_c}{h_p} \tag{39}$$

Since the temperature distributions in the membranes appeared to be the straight lines (Figs. 12–14), the heat conduction can be rewritten in the simple form below

$$q_c = k_m \left( \frac{T_1 - T_2}{\delta} \right) \tag{40}$$

From Fig. 6, $q_v$ slightly drops with decreasing temperature across the membrane. As a result, $q_v$ can be assumed constant at the average membrane temperature: $(T_1 + T_2)/2$, given by

$$q_v = JH_v\{T_m\} = JH_v \left\{ \frac{T_1 + T_2}{2} \right\} \tag{41}$$

After substituting Eqs. (40) and (41) into Eqs. (38) and (39), the expressions for evaluating the membrane surface temperatures are shown below

$$T_1 = T_f - \frac{JH_v\{(T_1 + T_2)/2\} + k_m\{(T_1 - T_2)/\delta\}}{h_f} \tag{42}$$

$$T_2 = T_p + \frac{JH_v\{(T_1 + T_2)/2\} + k_m\{(T_1 - T_2)/\delta\}}{h_p} \tag{43}$$

The temperature polarization coefficient can be obtained by the combination of Eqs. (1), (42) and (43) for the simple case of the same film heat transfer coefficients ($h_f = h_p = h$) [8], expressed as

$$\tau = \frac{1 - [2JH_v\{T_m\}/h(T_f - T_p)]}{1 + (2k_m/\delta h)} \tag{44}$$

where

$$T_m = \frac{T_f + T_p}{2}$$

Usually, the heat transfer model is arranged in the complicated forms [3,27] which cannot provide the clear picture of temperature polarization. Therefore, the alternative method is proposed in order to offer both simple calculation and better illustration of temperature polarization. Initially ($n = 0$), the membrane surface temperatures $T_{1,n=0}$ and $T_{2,n=0}$ are approximated by Eqs. (45) and (46). The number 2 in Eqs. (45) and (46) refers to the comparable importance of heat conduction and heat due to vapor flow. Subsequently, $T_{1,n=1}$ and $T_{2,n=1}$ are obtained by replacing $T_{1,n=0}$ and $T_{2,n=0}$ into Eqs. (47) and (48). The calculations are repeated until the differences between $T_{n+1}$ and $T_n$ are smaller than 0.01%.

$$T_{1,n=0} = T_f - \frac{2JH_v(T_f + T_p)/2}{h_f} \tag{45}$$

$$T_{2,n=0} = T_p + \frac{2JH_v(T_f + T_p)/2}{h_p} \tag{46}$$

$$T_{1,n+1} = T_f - \frac{JH_v\{(T_{1,n} + T_{2,n})/2\} + k_m\{(T_{1,n} - T_{2,n})/\delta\}}{h_f} \tag{47}$$

$$T_{2,n+1} = T_p + \frac{JH_v\{(T_{1,n} + T_{2,n})/2\} + k_m\{(T_{1,n} - T_{2,n})/\delta\}}{h_p} \tag{48}$$

### 4.4. The influence of the spacers

When the spacers are put in the flow channels, the mass fluxes were increased (compared to laminar flow at the same flow rates). Fig. 15 shows that the mass

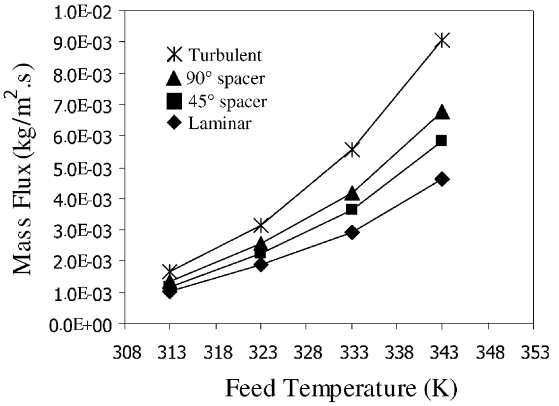


Fig. 15. Mass fluxes at various feed temperatures under laminar flow ($h = 1498.87\,W\,m^{-2}\,K^{-1}$), 90° spacer, 45° spacer, and turbulent flow ($17{,}026.3\,W\,m^{-2}\,K^{-1}$) for GVHP 0.22 μm.

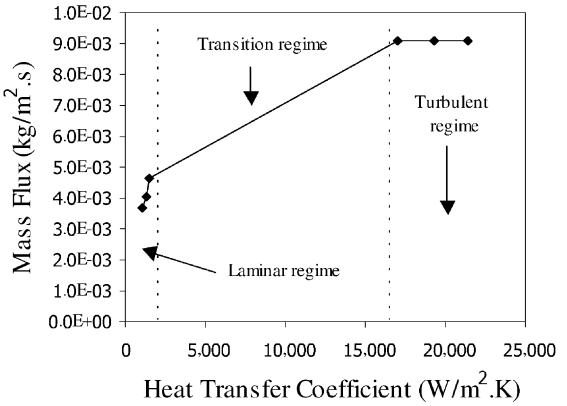


Fig. 16. Mass fluxes at various heat transfer coefficients for GVHP at 343 K.

fluxes enhanced by spacers were between the fluxes obtained from laminar and turbulent flow conditions. In addition, the mass fluxes increased by 90° spacers were higher than those increased by 45° spacers due to higher generated eddy [26] in 90° spacers. The mass fluxes enhanced by both spacers are much lower than those obtained from turbulent flow condition. Consequently, the flow characteristic of spacer-filled channels in DCMD was likely to be in the lower transition regime rather than turbulent regime. Compared to other membrane processes, the turbulent flow was obtained in RO and UF performed with spacers [9,11], and upper transition regime was found in UF with the zigzag spacers [10]. The flow characteristic in spacer-filled channel of UF was concluded to be the upper transition regime (close to turbulent flow) or turbulent flow. The difference in conclusions between DCMD and UF or RO can be explained by theory of high mass transfer rate convection to be mentioned in our next work.

Fig. 15 demonstrates that the values of the heat transfer coefficients for spacer-filled channels fell between those calculated by the correlations for laminar flow and turbulent flow or 1500–17,000 $W\,m^{-2}\,K^{-1}$ for the chosen correlations in this work, and can be estimated by Fig. 16. The preliminary calculations based on the assumption of constant MD coefficient gave the values of the heat transfer coefficients for spacer-filled channel in the range of 2000–5500 $W\,m^{-2}\,K^{-1}$. However, the heat transfer coefficients for spacer-filled channels in this work were considerably less than those calculated by Eq. (20) at the same Reynolds numbers.

## 5. Conclusions

The heat transfer model based on the simultaneous heat and mass transfer was used to identify the significance of each heat transfer mechanism and the influence of mass transfer on heat transfer rates. The theory of high mass transfer rate convection was used to assess the effect of mass transfer on heat transfer coefficients. The maximum effects of mass transfer on heat transfer rates in the feed and permeate streams were only 7.2 and 3.2%, respectively. The calculation results proved that the effects of mass transfer on heat transfer rates and on heat transfer coefficient can be neglected. The significance of heat conduction in the membranes and of heat transfer due to vapor flowing was comparable. The assumption of linear temperature profile inside the membranes and vapor flowing with constant enthalpy was valid for all membranes studied. The MD coefficients remained unchanged with the operating conditions employed in this work and depended only on the membrane properties. Therefore, the MD coefficient can be considered as the characteristic values for each membrane. In this work, the MD coefficients were $3.459 \times 10^{-7}$, $4.169 \times 10^{-7}$, and $6.245 \times 10^{-7}\,kg\,m^{-2}\,s^{-1}\,Pa^{-1}$ for GVHP, HVHP, and PTFE, respectively.

For the experiments with the spacers, 26–56% increase in mass fluxes were achieved, compared with the fluxes performed under laminar flow. Furthermore, the flow characteristic in the spacer-filled channels was likely to fall in the lower transition regime rather than the turbulent regime. The heat transfer coefficients for spacer-filled channels were estimated in the range of 2000–5500 $W\,m^{-2}\,K^{-1}$, or were enhanced by approximately 2.5 times of the heat transfer coefficients for laminar flow.

## Acknowledgements

The authors would like to thank The Thailand Research Fund and The Royal Golden Jubilee Ph.D. Program for financial support. J. Phattaranawik wishes to thank the UNESCO Centre for Membrane Science & Technology for hospitality.

## References

[1] R.B. Bird, W.E. Stewart, E.N. Lightfoot, Transport Phenomena, Wiley, New York, 1960.
[2] A.F. Mills, Mass Transfer, 2nd ed., Prentice-Hall, Englewood Cliffs, NJ, 2001.
[3] M. Gryta, M. Tomaszewska, Heat transport in membrane distillation process, J. Membr. Sci. 144 (1998) 211–222.
[4] M.A. Izquierdo-Gil, M.C. Garcia-Payo, C. Fernandez-Pineda, Air gap membrane distillation of sucrose aqueous solution, J. Membr. Sci. 155 (1999) 291–307.
[5] J. Phattaranawik, R. Jiraratananon, Direct contact membrane distillation: effect of mass transfer on heat transfer, J. Membr. Sci. 188 (2001) 137–143.
[6] K.W. Lawson, D.R. Lloyd, Membrane distillation. II. Direct contact MD, J. Membr. Sci. 120 (1996) 123–133.
[7] L. Martinez-Diez, M.I. Vazquez-Gonzalez, F.J. Florido-Diaz, Study of membrane distillation using channel spacers, J. Membr. Sci. 144 (1998) 45–56.
[8] J. Phattaranawik, R. Jiraratananon, A.G. Fane, C. Halim, Mass flux enhancement using spacer-filled channels in direct contact membrane distillation, J. Membr. Sci. 187 (2001) 193–201.
[9] A.R. Da Costa, A.G. Fane, C.J.D. Fell, A.C. M Franken, Optimal channel spacer design for ultrafiltration, J. Membr. Sci. 62 (1991) 275–291.
[10] J. Schwinge, D.E. Wiley, A.G. Fane, R. Guenther, Characterization of a zigzag spacer for ultrafiltration, J. Membr. Sci. 172 (2000) 19–31.
[11] G. Schock, A. Miquel, Mass transfer and pressure loss in spiral wound modules, Desalination 64 (1987) 339–352.
[12] R.W. Schofield, A.G. Fane, C.J.D. Fell, Heat and mass transfer in membrane distillation, J. Membr. Sci. 33 (1987) 299–313.
[13] E.A. Mason, A.P Malinauskas, in: S.W. Churchill (Ed.), Gas Transport in Porous Media: The Dusty-Gas Model, Elsevier, Amsterdam, 1983.
[14] R.W. Schofield, A.G. Fane, C.J.D. Fell, Gas and vapour transport though microporous membrane. II. Membrane distillation, J. Membr. Sci. 53 (1990) 173–185.
[15] J.M. Smith, H.C. Van Ness, Introduction to Chemical Engineering Thermodynamics, 4th ed., McGraw-Hill, New York, 1990.
[16] R.H. Perry, Perry's Chemical Engineers' Handbook, 6th ed., McGraw-Hill, New York, 1984.
[17] Y.K. Godovsky, Thermophysical Properties of Polymers, Springer, Berlin, 1992.
[18] A.B. Strong, Plastics: Material and Processing, 2nd ed., Prentice-Hall, Englewood Cliffs, NJ, 2000.
[19] J. Brandrup, E.H. Immergut, Polymer Handbook, 3rd ed., Wiley, New York, 1989.
[20] C.A. Harper, Handbook of Plastics, Elastomers and Composites, 3rd ed., McGraw-Hill, New York, 1996.
[21] D.W. Van Kreveleh, Properties of Polymers, 3rd ed., Elsevier, Amsterdam, 1990.
[22] C.L. Yaws, Handbook of Transport Property Data: Viscosity, Thermal Conductivity, and Diffusion Coefficients of Liquids and Gases, Gulf Publishing, Houston, 1995.
[23] S.B. Warner, Fiber Science, Prentice-Hall, Englewood Cliffs, NJ, 1995.
[24] S.M. Lee, International Encyclopedia of Composites, vol. 5, VCH Publishers, New York, 1991.
[25] A.R. Da Costa, A.G. Fane, D.E. Wiley, Ultrafiltration of whey protein solutions in spacer-filled flat channels, J. Membr. Sci. 76 (1993) 245–254.
[26] A.R. Da Costa, A.G. Fane, D.E. Wiley, Spacer characterization and pressure drop modeling in spacer-filled channels for ultrafiltration, J. Membr. Sci. 87 (1994) 79–98.
[27] M. Gryta, M. Tomaszewska, A.W. Morawski, Membrane distillation with laminar flow, Sep. Purif. Technol. 11 (1997) 93–101.
[28] E.N. Sieder, G.E. Tate, Heat transfer and pressure drop of liquid in tubes, Ind. Eng. Chem. 28 (1936) 1429–1435.
[29] L.C. Thomas, Heat Transfer, Prentice-Hall, Englewood Cliffs, NJ, 1992.
[30] K.P. Hagan, Heat Transfer with Application, Prentice-Hall, Englewood Cliffs, NJ, 1990.
[31] F.W. Dittus, L.M.K. Boelter, Publications on Engineering, vol. 2, University of California, Berkeley, 1930.
[32] M.N. Ozisik, Heat Transfer (A Basic Approach), McGraw-Hill, New York, 1985.
[33] S. Aravinth, Prediction of heat and mass transfer for fully developed turbulent fluid flow through tubes, Int. J. Heat. Mass Transfer 43 (2000) 1399–1408.
[34] J.R. Welty, C.E. Wicks, R.E. Wilson, Fundamentals of Momentum, Heat and Mass Transfer, 3rd ed., Wiley, New York, 1984.